An ultrasensitive detection of miRNA-155 in breast cancer via direct hybridization assay using two-dimensional molybdenum disulfide field-effect transistor biosensor

Samira Mansouri Majd, Abdollah Salimi, Foad Ghasemi

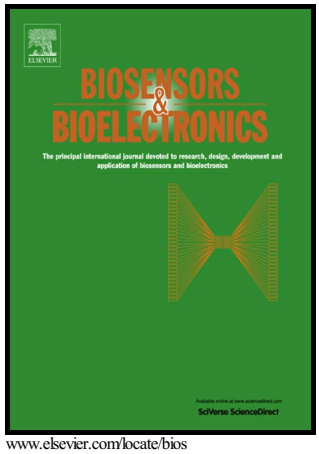

www.elsevier.com/locate/bios

PII: S0956-5663(18)30016-2
DOI: https://doi.org/10.1016/j.bios.2018.01.009
Reference: BIOS10202

To appear in: *Biosensors and Bioelectronic*

Received date: 20 October 2017
Revised date: 28 December 2017
Accepted date: 5 January 2018

Cite this article as: Samira Mansouri Majd, Abdollah Salimi and Foad Ghasemi, An ultrasensitive detection of miRNA-155 in breast cancer via direct hybridization assay using two-dimensional molybdenum disulfide field-effect transistor biosensor, *Biosensors and Bioelectronic,* https://doi.org/10.1016/j.bios.2018.01.009

An ultrasensitive detection of miRNA-155 in breast cancer via direct hybridization assay using two-dimensional molybdenum disulfide field-effect transistor biosensor

Samira Mansouri Majd,[a] Abdollah Salimi,[a,b*] Foad Ghasemi [c]

[a] Department of Chemistry, University of Kurdistan, 66177-15175, Sanandaj-Iran

[b] Research Center for Nanotechnology, University of Kurdistan, 66177-15175, Sanandaj-Iran

[c] Nanoelectronic Lab, School of Electrical and Computer Engineering University of Tehran, 14399-56191, Tehran-Iran

* Corresponding author. Tel: +9887333624001, Fax: +9887333624008

E-mail: absalimi@uok.ac.ir, absalimi@yahoo.com

Abstract: MicroRNAs (miRNAs), critical biomarkers of acute and chronic diseases, play key regulatory roles in many biological processes. As a result, robust assay platforms to enable an accurate and efficient detection of low-level miRNAs in complex biological samples are of great significance. In this work, a label-free and direct hybridization assay using molybdenum disulfide (MoS_2) field-effect transistor (FET) biosensor has been developed for ultrasensitive detection of miRNA-155 as a breast cancer biomarker in human serum and cell-line samples. MoS_2, the novel 2D layered material with excellent physical and chemical properties, was prepared through sequential solvent exchange method and was used as an active channel material. MoS_2 was comprehensively characterized by spectroscopic and microscopic methods and it was applied for fabrication of FET device by drop-casting MoS_2 flacks suspension onto the FET surface. MoS_2 FET device showed a relatively low subthreshold swing of 48.10 mV/decade and a high mobility of 1.98×10^3 $cm^2V^{-1}s^{-1}$. Subsequently, probe miRNA-155 strands were immobilized on the surface of the MoS_2 FET device. Under optimized conditionsdetection limit of 0.03 fM and concentration range 0.1 fM to 10 nM were achieved. The developed biosensor not only was capable to identification of fully matched versus one-base mismatch miRNA-155 sequence, but also it could detect target miRNA-155 in spiked real human serum and extracts from human breast cancer cell-line samples. This approach paves a way for label-free, early detection of miRNA as a biomarker in cancer diagnostics with very high sensitivity and good specificity, thus offering a significant potential for clinical application.

Key words: Two dimensions Molybdenum disulfide, Field-effect transistor, miRNA, Breast cancer, biosensor.

1. Introduction

Cancer is a public health concern worldwide and is known as one of the leading cause of death (Siegel et al., 2014). Breast cancer remains one of the top threats to the health of women and its early detection is the key to high potential, easy, inexpensive and most effective therapy (Caplan et al., 2014). Nowadays, current diagnostic tools that are normally used for the diagnosis of breast cancer are clinical and physical examinations, imaging mammography, ultrasound magnetic resonance imaging and histopathology. But some drawbacks such as insufficient results of clinical and physical examination, limited sensitivity and the risk of exposure to radiation for mammography, low sensitivity of safe and non-invasive ultrasound, especially in women above 40, and non-applicability of the histopathology in the early stages of disease have limited application of these approaches (Yahalom et al., 2013). Therefore, the development of non-invasive, simple and low risk approaches for screening/diagnosing breast cancer is essential. The use of serum biomarkers opens the possibility towards a simple serological test for prognosis/diagnosis and follow-up of breast cancer under therapy (Chung et al., 2014). In breast cancer, several serum markers (for example carbohydrate antigen 15-3, carcinoembryonic antigen, tissue polypeptide specific antigen) may be used in clinical practice, but carbohydrate antigen 15-3 (CA 15-3) was the most widely used serum biomarker. However, it cannot be used exclusively due to its lack of sensitivity at an early stage of the disease (Sun et al., 2012). One major impediment to improving the management of breast cancer is the current lack of tumor marker with sufficient sensitivity and specificity. In this route, emerging novel biomarkers like microRNAs have made great promises (Nana-Sinkam and Croce, 2013).

MicroRNAs are a class of single strand, regulation of gene expression, small and short non-coding RNAs with 18-24 nucleotides in length (Johnson and Mutharasan, 2014). They associate

with an RNA-induced silencing complex and regulate the expression of target genes at the post-transcriptional level by either translational repression or degradation of messenger RNA (mRNA) (Ambros, 2004). MicroRNAs play an essential role in biological processes such as development, cellular proliferation, apoptosis and response to stress, and tumorigenesis. Aberrant miRNA expression levels have been implicated as a biomarker in several different forms of disease including several types of cancer (Lawrie et al., 2008), cardiovascular disorders (Edwards et al., 2010), diabetes (Nielsen et al., 2012), rheumatic diseases (Alevizos and Illei, 2010), and neurological disorders (Miller and Wahlestedt, 2010), kidney disease (De Planell-Saguer and Rodicio, 2013), liver disease (Bernardo et al., 2012) and even immune dysfunction (Nalejska et al., 2014). In breast cancer, several studies have supported an abnormal expression of miRNA-155 in patients with the disease (Mattiske et al., 2012). miRNA-155 as an important circulating miRNA, is a robust oncogenic miRNA which its overexpression plays a significant role in the process of carcinogenesis and can be used as a biomarker for diagnosis, staging, progression and prognosis of the cancers (Zhang et al., 2009). To date, several approaches have been developed for miRNA detection, including conventional techniques (such as northern blot analysis (Valoczi et al., 2004), real-time quantitative polymerase chain reaction (Li et al., 2009), microarrays (Lee and Jung, 2011), molecular cloning (Takada et al., 2006)) and relatively recent advancements (electrochemical-based and optical-based biosensors) (Liao et al., 2016).

Among sensing methods, transistor-based sensors have been proposed as one of the most promising biomedical technologies and devices since they can be used as core sensing components (Karnaushenko et al., 2015, Mansouri Majd et al., 2017). The label-free FET biosensors do not have limitations of conventional techniques and also they do not require electrochemical or fluorescent tags. Due to their intrinsic amplification and rapid and label free

detection, they can detect a variety of target analytes sensitively and selectively via efficient interfacial transfer of charge carriers (Cai et al., 2015). The main challenge in FET structure is the development of the active channel layer that in addition to picking up the receiver operating environment, offers satisfactory electronic performance.

Various materials can be applied to transducers in liquid-ion gated FET. Recent works have reported FETs based on one-dimensional (1D) and two-dimensional (2D) nanostructures such as nanowires, nanotubes, nanobelts and nanosheets (Chen et al., 2017). The richness of the electrical, optical, and mechanical properties of two-dimensional materials has stimulated tremendous scientific enthusiasm and industrial development (Sim et al., 2015). As a result, an increasing amount of attention has been diverted to potential 2D materials, such as atomically layered transition metal dichalcogenides (TMDCs) for sensor applications due to their electron- and proton- accepting behavior. In particular, molybdenum disulfide, one of the most stable TMDCs, is a layered semiconductor with weak interplanar van der waals interactions that has a large surface-to-volume ratio, good carrier mobility, and a low noise level (An and Jang, 2017). MoS_2 undergoes a direct-to-indirect and wide-to-narrow band-gap transition as its structure changes from a single layer to a bulk crystal. More recently, many studies on MoS_2 have fully illustrated its enormous potential for use in the fabrication of electronic components, field-effect transistors, gas or pressure sensors, optical detectors and capacitors (Li et al., 2017). Also some MoS_2-based biosensors for protein or DNA have been reported (Sarkar et al., 2014). DNA-functionalized MoS_2 nanosheet/gold nanoparticle hybrid FET sensor applied for the ultrasensitive detection of Hg^{2+} in an aqueous environment (Zhou et al., 2016). Furthermore, a label-free sensitive biosensor platform using multi-layer MoS_2 FET devices developed for prostate-specific antigens (PSA) detection (Wang et al., 2014).

In this study, by integration of the advantages of the MoS_2 and label-free FET, an efficient biosensor has been achieved for miRNA-155 detection in breast cancer sensitively and selectively. Initially, the sensing layer of MoS_2 was prepared through sequential solvent exchange method and then MoS_2 flacks suspension was drop-casted onto the FET surface. For fabrication of biosensor, probe miRNA-155 strands were immobilized onto the MoS_2 via physically adsorb on the basal plane of MoS_2. In the detection, the complementary target miRNA-155 strands were hybridized to probe miRNA-155 strands and double-stranded miRNA-155 conjugates were desorbed from the MoS_2 channel and were lead to the current increase in the MoS_2 FET biosensor. This biosensor was able to detect target miRNA-155 precisely in low concentration while very low responses observed for one-base mismatch sequences. The application of the biosensor for target miRNA-155 measuring was successfully evaluated in human serum and cell-line samples.

2. Experimental Section

2.1. Materials and Reagents

MoS_2 powders (with flake sizes between 3 and 40 μm, purity of 99%) and N-Methyl-2-pyrrolidone (NMP) were purchased from Sigma Aldrich. N, N-dimethylformamide (DMF) and isopropyl alcohol (IPA) solvents were supplied from Merck Company and no special purification was performed. All miRNA-155 sequences were purchased from BIONEER, Global Genomics Partner and purified using HPLC. The sequences were as follows:

Probe miRNA-155 (probe strand that was amino modified with adenine spacers): 5'-NH_2-AAA AAA AAC CCC UAUCAC GAU UAG CAU UAA-3'

Target miRNA-155 (complementary strand): 5'-UUA AUG CUA AUC GUG AUAGGG GU-3'

One-base mismatch miRNA-155 strand: 5'-UUA AUG CUA CUC GUG AUAGGG GU-3'

Human serum samples for real sample analysis were supplied by a clinical diagnostic laboratory. The human breast cancer cell line MCF-7 was obtained from the national cell bank of Iran (Pasteur institute of Iran, Tehran) and was cultured by established protocols (the details for other materials and cell culture and total miRNA-155 extraction were reported in Supporting Information (SI)).

2.2. Instruments

The details of instruments used for electrical, optical and microscopic measurements were reported in SI.

2.3. Preparation of MoS_2 nanosheets

MoS_2 nanosheets were prepared based on the phase liquid exfoliation (Ghasemi et al., 2016). The details of the synthesis process reported in SI.

2.4. Fabrication of MoS_2 FET biosensor

Figure S1 (SI) showed schematic diagrams of the fabrication process on a Si substrate. The FET fabrication process was started with thermally grown 285 nm thick SiO_2 on p-type silicon substrate, referred to as Si/SiO_2. Then, 5 nm Ti and 50 nm gold were deposited on Si/SiO_2 substrates by means of a radio frequency (13.56 MHz) sputtering unit. A microarray, consisting of 11 pairs of interdigitated microelectrodes, was patterned on a Si/SiO_2 substrate via a photolithographic process, resulting in electrodes with a width of 4 µm, length of 40 µm, and an inter-electrode spacing of 4 µm. The oxide layer acts as a back gate oxide for this structure while the Au/Ti interdigital features act as source and drain electrodes (Fig S.2). To make contact to the silicon back gate, the SiO_2 layer has been etched away in a buffered HF solution in desired regions. Then 10 µL of as-prepared few-layer MoS_2 flakes were drop-casted on the pre-patterned electrodes following by drying at 70 °C. Finally, device was incubated with 20 µL of probe

miRNA-155 strands solution (1μM in 0.01 PBS with pH 7.4) for 18 h in 4 °C. Part A of schematic 1 at left side demonstrates the fabricated biosensor and SEM image at right side demonstrates few-layer MoS_2 on the surface electrodes.

3. Results and discussion

3.1. Characterization of MoS_2 nanosheets

MoS_2 nanosheets were first imaged by AFM to determine the sample thickness (Fig. 1a). The height profile taken along the 5μm white line in the AFM image showed a thickness of 2-4 nm for nanosheets (Fig. 1b). Interlayer spacing for MoS_2 single layer of the S-Mo-S building block of the MoS_2 crystal is 0.62 nm (Splendiani et al., 2010). Thus, in our sample, each sheet was composed of ~3-6 layers of MoS_2 molecular sheets. As seen in Figure 1c, the TEM image of nanosheets demonstrated transparent layers and it confirmed the formation of MoS_2 nanosheets in which sample contained few layers with large surface area. Moreover, no trace of re-aggregation or porous structure was observed in the TEM image of nanosheets which showed no special deformation of layers due to exposing to O_2 plasma. Figure 1d showed the Raman spectral analysis of MoS_2 nanosheets. As shown in Figure 1d, Raman studies of MoS_2 nanosheets exhibited two characteristic peaks at 385 cm^{-1} and 404 cm^{-1} that were correspond to the E^1_{2g} (in-plane) attributed to the opposite vibration of two S atoms with respect to Mo and A_{1g} (out-of-plane) vibration of only S atoms in opposite directions. A_{1g} mode is very sensitive to adsorbates on the MoS_2 surface and charge exchanges due to its out-of-plane nature (Srinivasan et al., 2016). The number of MoS_2 layers was also confirmed by Raman spectroscopy based on the peak spacing between the E^1_{2g} mode and the A_{1g} mode. Spatial maps of the Raman frequency for the A_{1g} and E^1_{2g} modes (insets of Figure 2d) clearly demonstrate that the frequencies of the two modes have only very slight variation for different locations within a sample of a given layer

thickness. This permits the Raman frequencies to be used as an indicator of the layer thickness. The frequency difference of 19 cm^{-1} between the E^1_{2g} and A_{1g} modes in the Raman spectra supported the successful acquisition of few layer MoS_2 (~ between 3 to 6 layers) via the phase liquid exfoliation method (Castellanos-Gomez et al., 2012). In order to confirm MoS_2 successful synthesis, X-Ray diffraction analysis was conducted. XRD pattern of MoS_2 was shown in Figure S3. The characteristic peaks clearly confirmed the 2H-MoS_2 structure with d-spacing 6.17Å of (002) diffraction peak (Cheng et al., 2016). Compared with the pristine pattern, our MoS_2 possessed the same peaks with lower intensity indicating some degree of exfoliation by O_2 plasma while no specific peaks were identified for MoO_2 or MoO_3 structures. Moreover, a shift in the peaks towards lower angles might be assigned to the presence of smaller sheets which in the case of (002) direction, the d-spacing shifts to 6.18 Å showing a slight expansion of interlayer distance (Fan et al., 2015). Therefore, low intensity and shifted peaks were believed to result from slight exfoliation of sheets for O_2-MoS_2 in comparison with the pristine MoS_2 (Cheng et al., 2016; Fan et al., 2015; Su et al., 2015). The UV-Vis spectrum and PL spectral analysis of the MoS_2 nanosheets were presented in Figure 1e and 1f, respectively. As shown in Figure 1e, the prepared MoS_2 nanosheets showed a two absorption peaks at 610 and 670 nm. The peaks at 610 and 670 nm which are attributed to direct transition from the valance band to the conduction band at the K-point of the Brillouin zone, known as the B and A transitions which indicate the existence of layered MoS_2 dispersed in the solvent (Deng et al., 2015). Similarly, MoS_2 nanosheets had two characteristic emission peaks (Fig. 1f) at 620 and 680 nm for 500 nm excitation wavelength which were correlated to the B and A direct excitonic transitions from the lowest conduction band to the highest spin–split valence band at the K-point of the Brillouin zone (Eda et al., 2011).

3.2. Electrical measurements

The electrical characterization of the device was first carried out in dry environment by measuring the transfer characteristics as a function of drain and back gate voltages. Figure 2a,b showed family curves of drain current-drain voltage (I_d-V_d) at different back gate voltage (from 0.0 V to 4.0 V with 1.0V step) and drain current-back gate voltage (I_d-$V_{back\ gate}$) with drain voltage fixed at 0.1 V, respectively. The output characteristics of the FET devices illustrated n-type transistor behavior with good saturation, and the MoS_2 FET showed high field-effect mobility (μ) of 1.98×10^3 $cm^2V^{-1}s^{-1}$ and on/off ratios (I_{on}/I_{off}) 7.12×10^2 and low subthreshold swing (SS) 48.10 mV/decade.

For biosensing applications, it is necessary that these devices can be operated in a wet environment. Hence, the devices were measured in a wet environment by transferring electrolyte solution (0.01 M PBS) to the surface of the active channel material. The performance of MoS_2 FETs was shown in Figure 2c (I_d-V_d curves at different back gate voltage from 0.0 V to 5.0 V with 1.0V step) and 2d (I_d-$V_{back\ gate}$ curves with drain voltage fixed at 0.1 V). They illustrated that the biosensor device was efficiently controlled in the wet environment, and the MoS_2 FETs had good FET behavior with low driving voltage.

3.3. Sensitivity of the biosensor toward complementary miRNA-155 strands

Electrical measurements on the hybridization of target miRNA-155 strands with the probe miRNA-155 strands were carried out for the FET with a MoS_2 channel in the electrolyte. The lack of dangling bonds on the MoS_2 basal plane makes the immobilization of probe miRNA-155 molecules through covalent bonding or other strong bonds difficult. However, nucleobases of probe miRNA-155 strands can interact with the basal plane of MoS_2 through van der Waals forces (Zhu et al., 2013). For example, physical adsorption of aromatic and conjugated

compounds on the basal plane of MoS_2 was demonstrated theoretically and experimentally (Moses et al., 2009). When the probe miRNA-155 strands were immobilized on the basal plane of the MoS_2 channel, the transfer characteristics of the device changed significantly. The I_d at V_d = 0.1 V was significantly reduced (Fig. 3a). These effects can be explained by the electrostatic gating effects. The probe miRNA-155 strands physically adsorbed on the basal plane of MoS_2 are negatively charged due to their phosphate backbone. The negative charges of the adsorbed probe miRNA-155 on the n-type MoS_2 channel reduce the effective gate field under a positive gate biasing condition and, as a result, reduce the density of the accumulated electrons. This, in turn, reduces the I_d. Schematic 1B at left side also depicted this phenomenon.

Measurements of the transfer characteristics of miRNA-155 hybridization were carried out by adding complementary miRNA-155 strands on the FET functionalized with the probe miRNA-155. The transfer characteristics during measurements were obtained by applying $V_{back\ gate}$ from 0.0 to 1.0 V at a V_d of 0.1 V. When the complementary miRNA-155 with a concentration ranging from 0.1 fM to 10 nM was added and hybridized with the probe miRNA-155 strands, the I_d increased, i.e. closer to the transfer curve of the pristine MoS_2 FET (Fig. 3a). The results indicated the reduction of negative charges, which was attributed to desorption of hybridized, double-stranded miRNA-155 conjugates from the MoS_2 channel due to their decreased binding force (Lee et al.,2015). This desorption increased effective gate field and reduced charge scattering in the MoS_2 channel (schematic 1B at right side).

The sensitivity was determined from percentage of normalized drain current change at fixed V_d=0.1 V and $V_{back\ gate}$=1.0V (Fig. 3b). The device was incubated with 20 µl of each concentration of complementary miRNA-155 for 40min optimized incubation time (Fig. S4). The current increased linearly upon increasing complementary miRNA-155 concentration,

indicating that the response was the direct result of complementary target miRNA-155 hybridization with probe miRNA-155. The limit of detection (LOD) calculated using the 3σ/S approach (Chen et al., 2016) was 0.03 fM, (signal-to-noise: 3.1). The various methods for miRNA-155 sensing based on probe miRNA-155 hybridization were illustrated in Table 1. Compared with other label-free miRNA-155 detection methods (except the method performed by Cardoso et al.), the MoS_2 FET-based biosensor had lower limit of detection and wider linear range.

3.4. Selectivity measurements

The specificity of the response to complementary miRNA-155 was evaluated by monitoring of I_d in various solutions containing one-base mismatch miRNA-155 strands (Fig. 3c). When one-base mismatch miRNA-155 strands with a concentration ranging from 0.1 fM to 1 pM were added, the I_d value did not vary significantly (Fig. 3c and 3d). As can be seen from Figure 3b,d, sensitivity of miRNA-155 hybridization in the MoS_2 FET was found to be 10.976 1/decade at a large dynamic range that was more than sensitivity of one-base mismatch miRNA-155 hybridization (1.847 1/decade). The result suggested that the proposed assay had excellent base discrimination capability. Also, the selectivity of the biosensor toward complementary miRNA-155 was evaluated by measuring the current of the proposed FET for various interfering species commonly found in biological fluids, including CEA (1.0×10^{-2} ng/mL), BSA (1.0×10^{3} ng/mL) and CA15-3 (1×10^{-6} U/mL) compared to complementary miRNA-155 (1×10^{-13} M) (Fig. S5a). As can be seen in recorded chart bars in Fig. S5b, the current decrease for CA15-3 (1.0 μA), CEA (0.97 μA) and BSA (1.62 μA) was significantly smaller than the current increase caused by complementary miRNA-155 with respect to blank (-9.98 μA). The specificity results further confirm that the biosensor response comes from the hybridization of complementary miRNA-

155 with complementary miRNA-155. Also, the very low response of the aptasensor to interfering species is due to some non-specific interaction with MoS_2.

3.5. Real sample analysis

In order to further investigate the practical application of the MoS_2 FET-type biosensor, we challenged miRNA-155 detection in real samples. Healthy human serum was used as real sample. At first healthy human serum was diluted 10-fold with PBS and then three different concentrations of complementary miRNA-155 (10^{-14}, 10^{-15} and 10^{-16} M) were spiked into the serum 10-fold-diluted and detected for 3 times. A blank control test with 10-fold-diluted serum without any miRNA-155 was performed (Fig. 4a). As shown in Figure 4a, in 10-fold-diluted serum sample (healthy serum), the biosensor still maintained high detection ability and I_d had little increase with respect to obtained I_d for biosensor in PBS and for three different spiked concentrations of complementary miRNA-155, I_d increased with complementary miRNA-155 concentration increase. A histogram details the sensing performance of the MoS_2 FET at $V_{back\ gate}$=1.0V for Figure 4a diagram was shown in Figure 4b (blue columns). The blue columns of Figure 4b showed that change in I_d (ΔI) increased with complementary miRNA-155 concentration increase from 10^{-16} M to 10^{-14} M in serum sample and the sensitivity was 1.282 μA/decade (the dashed line). For comparison, we showed obtained responses of biosensor (ΔI) for the same concentrations of complementary miRNA-155 in buffer (PBS) (red columns in Figure 4b). When complementary miRNA-155 concentration in PBS was increased from 10^{-16} M to 10^{-14} M, ΔI increased and the sensitivity was 1.825 μA/decade (the continuous line). The results demonstrated that the biosensor still works well in serum samples, showing its potential of being applied in the practical applications.

To evaluate the feasibility of the biosensor for real sample detection, the expression of miRNA-155 in human breast cancer MCF-7 cell-lines was also investigated using the proposed biosensor. As shown in Figure 4c, the drain current increased when the cells amount increased from 25000 to 45000 cells. Figure 4d showed that normalized current change percentage increased linearly via the increased cell concentration. Thus, the proposed biosensor can be employed to detect miRNA-155 in cancer cells.

3.6. Reproducibility and storage stability

Four devices were employed to detect miRNA-155 (10^{-12} M) three times under the same condition to test the reproducibility of the proposed biosensor. The biosensor showed response with a relative standard deviation (RSD) below 3.5%. These experimental results indicated that the proposed sensor has good reproducibility. Storage stability of the presented biosensor was assessed in ambient condition and after 8 weeks of storage, the FET biosensor retains about 94% of its original response for 10^{-12} M miRNA-155. These results indicate acceptable reproducibility and stability of the proposed miRNA-155biosensor.

4. Conclusions

In summary, we have demonstrated a highly sensitive FET biosensor to detect miRNA-155 in serum and cell line samples based on the novel two dimensions MoS_2, whose semiconducting nature together with the prowess of its 2D layered structure makes it highly advantageous for biosensing. Few layer MoS_2 nanosheets were readily prepared through simple sequential solvent exchange method process. The nanosheets structure of the MoS_2 provided a large specific surface area, which enabled the loading of a considerable number of probe miRNA-155 strands. The results indicated that the MoS_2 FET biosensor can be used to detect target miRNA-155 strands with a low detection limit of 0.03 fM in a linear range from 0.1 fM to 10.0 nM with

high sensitivity 10.976 1/decade. We evaluated good specificity toward complementary miRNA-155 strands by characterizing the response of the biosensor in solutions containing one-base mismatch strands. We further demonstrated tests using spiked complementary miRNA-155 strands in 10-fold diluted healthy human serum with linear responses and the biosensor was able to detect very low concentrations of miRNA-155, down to 0.1 fM in a serum background. Extracts from MCF-7 cell-lines from breast cancer were also analyzed, yielding a positive signal against miRNA-155. Our findings demonstrated this label-free, ultrasensitive and selective MoS_2 FET biosensor can be a promising approach for quantitative analysis of miRNA-155 in physiological fluids and point-of-care diagnosis.

Acknowledgments: This research was supported by the Iranian Nanotechnology Initiative and the Research Offices of the University of Kurdistan (grant number 4.1404086).

References

Alevizos, I., Illei, G. G., 2010. Nat. Rev. Rheumatol. 6, 391-398.

Ambros, V., 2004. Nature 431, 350-355.

An, J. H., Jang, J., 2017. Nanoscale 9, 7483-7492.

Azimzadeh, M., Rahaie, M., Nasirizadeh, N., Ashtari, K., Naderi-Manesh, H., 2016. Biosens. Bioelectron. 77, 99-106.

Bernardo, B.C., Charchar, F. J., Lin, R. C. Y., McMullen, J. R., 2012. Heart Lung Circ. 21, 131-42.

Cai, B., Huang, L., Zhang, H., Sun, Z., Zhang, Z., Zhang, G. J., 2015. Biosens. Bioelectron. 74, 329-334.

Caplan, L., 2014. Front. Public Health 2, 1-5.

Cardoso, A. R., Moreira, F. T. C., Fernandes, R., Goreti, M., Sales, F., 2016. Biosens. Bioelectron. 80, 621-630.

Castellanos-Gomez, A., Barkelid, M. A., Goossens, M., Calado, V. E., Van der Zant H. S. J., Steele, G. A., 2012. Nano Lett. 12, 3187-3192.

Chen, H., Chen, P., Huang, J., Selegard, R., Platt, M., Palaniappan, A., Aili, D., Iing, A., Tok, Y., Liedberg, B., 2016. Anal. Chem. 88, 2994-2998.

Chen, H., Rim, Y. S., Wang, I. C., Li, C., Zhu, B., Sun, M., Goorsky, M. S., He, X., Yang, Y., 2017. ACS Nano 11, 4710-4718.

Cheng, P., Sun, K., Hu, Y. H., 2016. Nano. Lett. 16, 572-576.

Chung, L., Moore, K., Phillips, L., Boyle, F. M., Marsh, D. J., Baxter, R. C., 2014. Breast Cancer Research : BCR, 16(3), R63.

Deng, H., Yang, X., Gao, Z., 2015. Analyst 140, 3210.

De Planell-Saguer, M., Rodicio, M. C., 2013. Clin. Biochem. 46, 869-878.

Eda, G., Yamaguchi, H., Voiry, D., Fujita, T., Chen, M., Chhowalla, M., 2011. Nano Lett. 11, 5111.

Edwards, J. K., Pasqualini, R., Arap, W., Calin, G. A., 2010. J. Cardiovasc. Transl. Res. 3, 271-279.

Fan, X., Xu, P., Zhou, D., Sun, Y., Li, Y. C., Nguyen, M. A. T., Terrones, M., Mallouk, T. E., 2015. Nano. Lett. 15, 5956-5960.

Ghasemi, F., Mohajerzadeh, S., 2016. ACS Appl. Mater. Interfaces 8, 31179-31191.

Johnson, B. N., Mutharasan, R., 2014. Analyst 139, 1576.

Karnaushenko, D., Munzenrieder, N., Karnaushenko, D. D., Koch, B., Meyer, A. K., Baunack, S., Petti, L., Troster, G., Makarov, D., Schmidt, O. G., 2015. Adv. Mater. 27, 6797-6805.

Lawrie, C. H., Gal, S., Dunlop, H. M., Pushkaran, B., Liggins, A. P., Pulford, K., Banham, A. H., Pezzella, F., Boultwood, J., Wainscoat, J.S., Hatton, C.S., Harris, A.L., 2008. Br. J. Haematol. 141, 672-675.

Lee, D.W., Lee, J., Sohn, Y., Kim, B.Y., Son, Y. M., Bark, H., Jung, J., Choi, M., Kim, T.H., Lee, C., Lee, N.E., 2015. Nano Research 8, 2340-2350.

Lee, J. M., Jung, Y., 2011. Angew. Chem. Int. Ed. Engl. 50, 12487-12490.

Li, J., Yao, B., Huang, H., Wang, Z., Sun, C., Fan, Y., Chang, Q., Li, S., Wang, X., Xi, J., 2009. Anal. Chem. 81, 5446-5451.

Li, M., Liu, N., Li, P., Shi, J., Li, G., Xi, N., Wang, Y., Liu, L. 2017. ACS Appl. Mater. Interfaces 9, 8361-8370.

Liao, R., He, K., Chen, C., Cai, C., Chen, X., 2016. Anal. Chem. 88, 4254-4258.

Mansouri Majd, S., Salimi, A., Asteinchap, B., 2017. Biosens. Bioelectron. 92, 733-740

Mattiske, S., Suetani, R. J., Neilsen, P. M., Callen, D. F., 2012. Cancer Epidemol. Biomark. 21, 1236-1243.

Miller, B. H., Wahlestedt, C., 2010. Brain Res. 1338, 89-99.

Moses, P. G., Mortensen, J. J., Lundqvist, B. I., Norskov, J. K., 2009. J. Chem. Phys. 130, 104709.

Nalejska, E., Maczynska, E., Lewandowska, M. A., 2014. Mol. Diagn. Ther. 18, 273-284.

Nana-Sinkam, S.P., Croce, C.M., 2013. Clin. Pharmacol. Ther. 93, 98-104.

Nielsen, L. B., Wang, C., Sorensen, K., Bang-Berthelsen, C. H., Hansen, L., Andersen, M. L., Sarkar, D., Liu, W., Xie, X., Anselmo, A. C., Mitragotri, S., Banerjee, K., 2014. ACS Nano 8, 3992-4003.

Siegel, R., Ma, J., Zou, Z., Jemal, A., 2014. CA: Cancer J. Clin. 64, 9-29.

Sim, D. M., Kim, M., Yim, S., Choi, M. J., Choi, J., Yoo, S., Jung, Y. S., 2015. ACS Nano 9, 12115-12123.

Splendiani, A., Chim, C. Y., Sun, L., Galli, G., Zhang, Y., Wang, F., Li, T., Kim. J., 2010. Nano Lett. 10, 1271-1275.

Srinivasan, K., Subramanian, K., Murugan, K., Dinakaran, K., 2016. Analyst 141, 6344-6352.

Su, D., Dou, S., Wang, G., 2015. Adv. Energy Mater. 5, 1401205-1401211.

Sun, Y., Wang, M., Lin, G., Sun, S., Li, X., Qi, J., Li, J., 2012. PLoS ONE, 7, 1-8.

Takada, S., Berezikov, E., Yamashita, Y., Lagos-Quintana, M., Kloosterman, W. P., Enomoto, M., Hatanaka, H., Fujiwara, S., Watanabe, H., Soda, M., Choi, Y. L., Plasterk, R. H., Cuppen, E., Mano, H., 2006. Nucleic. Acids. Res. 34, 115.

Valoczi, A., Hornyik, C., Varga, N., Burgyan, J., Kauppinen, S., Havelda, Z., 2004. Nucl. Acids Res. 32, 175.

Wang, L., Wang, Y., Wong, J. I., Palacios, T., Kong, J., Yang, H. Y., 2014. Small 10, 1101-1105.

Wu, X., Chai, Y., Yuan, R., Su, H., Han, J., 2013. Analyst 138, 1060-1066.

Wu, X., Chai, Y., Yuan, R., Zhuo, Y., Chen, Y., 2014. Sens. Actuators B: Chem. 203, 296-302.

Yahalom, G., Weiss, D., Novikov, I., Bevers, T. B., Radvanyi, L. G., Liu, M., Piura, B., Iacobelli, S., Sandri, M. T., Cassano, E., Allweis, T. M., Bitterman, A., Engelman, P., Vence, L. M., Rosenberg, M. M., 2013. Biomarkers in Cancer, 5, 71-80.

Zhang, Y., Li, M., Wang, H., Fisher, W. E., Lin, P. H., Yao, Q., Chen, C., 2009. World J. Surg. 33, 698-709.

Zhou, G., Chang, J., Pu, H., Shi, K., Mao, S., Sui, X., Ren, R., Cui, S., Chen, J. 2016. ACS Sens. 1, 295-302.

Zhu, C., Zeng, Z., Li, H., Li, F., Fan, C., Zhang, H., 2013. J. Amer. Chem. Soc. 135, 5998-6001.

Zhu, W., Su, X., Gao, X., Dai, Z., Zou, X., 2014. Biosens. Bioelectron. 53, 414-419.

Figure captions

Table 1 Comparison of analytical performance of microRNA-155 detection platforms.

Scheme 1 (A) Schematic illustration for MoS_2 FET biosensor(left) and SEM image of MoS_2 onto the surface of the electrodes (right). (B) Schematic illustration for probe miRNA-155 strands immobilization (left) and complementary target miRNA-155 hybridization (right).

Figure 1 (a) AFM image of MoS_2 nanosheets. (b) The height profile taken along the 5μm white line in the AFM image. (c) TEM image of MoS_2 nanosheets (scale bar is 100nm). (d) Raman spectra of MoS_2 nanosheets (Inset shows spatial maps of the Raman frequency for the A_{1g} and E^1_{2g} modes). (e) UV-Vis and (f) PL spectra of MoS_2 nanosheets.

Figure 2 (a) I_d-V_d transfer curves of the the MoS_2 FET device at different biases of $V_{back\ gate}$ from 0 V to 4 V in 1 V steps (V_d: 0.0 to 2.0 V) measured in dry environment. (b) I_d-$V_{back\ gate}$ in Logarithmic scale (left) and I_d-$V_{back\ gate}$ (right) transfer curves of the MoS_2 FET obtained at a V_d of 0.1 V ($V_{back\ gate}$: 0.0 to 2.0 V) measured in dry environment. (c) I_d-V_d transfer curves of the the MoS_2 FET device at different biases of $V_{back\ gate}$ from 0 V to 5 V in 1 V steps (V_d: 0.0 to 1.0 V) measured in wet environment of 0.01 M PBS with pH 7.4. (d) I_d-$V_{back\ gate}$ in Logarithmic scale

(left) and I_d-$V_{back\ gate}$ (right) transfer curves of the MoS_2 FET obtained at a V_d of 0.1 V ($V_{back\ gate}$: 0.0 to 1.0 V) measured in wet environment of 0.01 M PBS with pH 7.4.

Figure 3 (a) I_d-$V_{back\ gate}$ responses for incubation of probe miRNA-155 strands with MoS_2 and then incubation of different concentrations of target miRNA-155 strands with increasing concentration from 10^{-16} M to 10^{-8} M measured in PBS (pH 7.4, 0.01M) at V_d= 0.1 V and their corresponding calibration curve (b). (c) I_d-$V_{back\ gate}$ responses for incubation of probe miRNA-155 strands with MoS_2 and then incubation of different concentrations of one-base mismatch miRNA-155 strands with increasing concentration from 10^{-16} M to 10^{-12} M in PBS (pH 7.4, 0.01M) at V_d= 0.1 V and their corresponding calibration curve (d).

Figure 4 (a) I_d-$V_{back\ gate}$ responses for incubation of probe miRNA-155 strands, 10-fold diluted human serum sample and different concentrations of target miRNA-155 strands spiked in 10-fold diluted human serum sample with increasing concentration from 10^{-16} M to 10^{-14} M at V_d= 0.1 V. (b) A histogram details the sensing performance of the MoS_2 FET at $V_{back\ gate}$=1.0V for (a) diagram and their corresponding calibration curve based on current difference and comparison of these results with obtained results for the same concentrations from measuring in PBS condition in figure 3a. (c) I_d-$V_{back\ gate}$ responses for incubation of different concentrations of extracted miRNA-155 from different numbers of cell line MCF-7 with increasing cell from 25000 cells to 45000 cells at V_d= 0.1 V and (d) their corresponding calibration curve.

Table 1 Comparison of analytical performance of microRNA-155 detection platforms.

Method	Detection limit	Linear range	Reference
Electrochemical impedance spectroscopy	5.7 aM	10 aM-1.0 nM	Cardoso et al., (2016)
Amperometry	1.87 pM	5.6 pM-0.56 µM	Wu et al., (2013)
Differential pulse voltammetry	0.6 fM	2 fM–8 pM	Azimzadeh et al., (2016)
Differential pulse voltammetry	3.3 fM	10 fM–1 nM	Wu et al., (2014)
Square wave voltammetry	12 fM	50 fM–30 pM	Zhu et al., (2014)
MoS_2 field-effect transistor	0.03 fM	0.1 fM-10 nM	This work

A

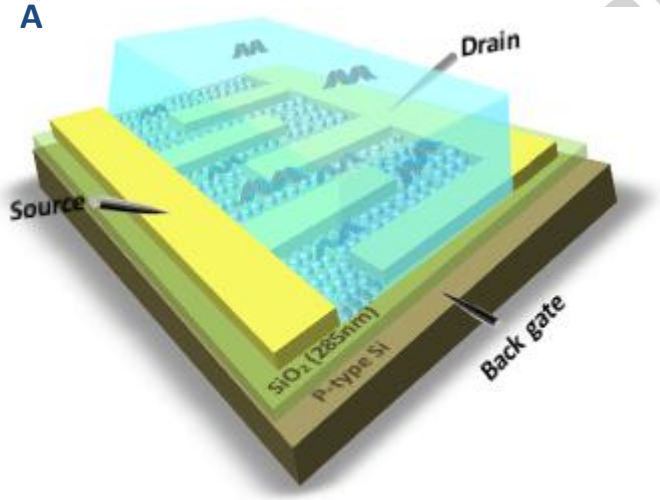

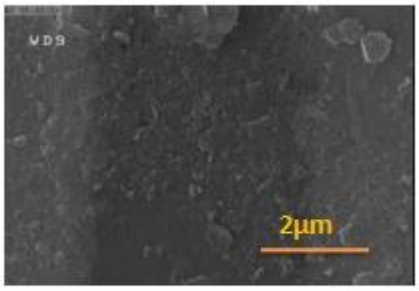

B

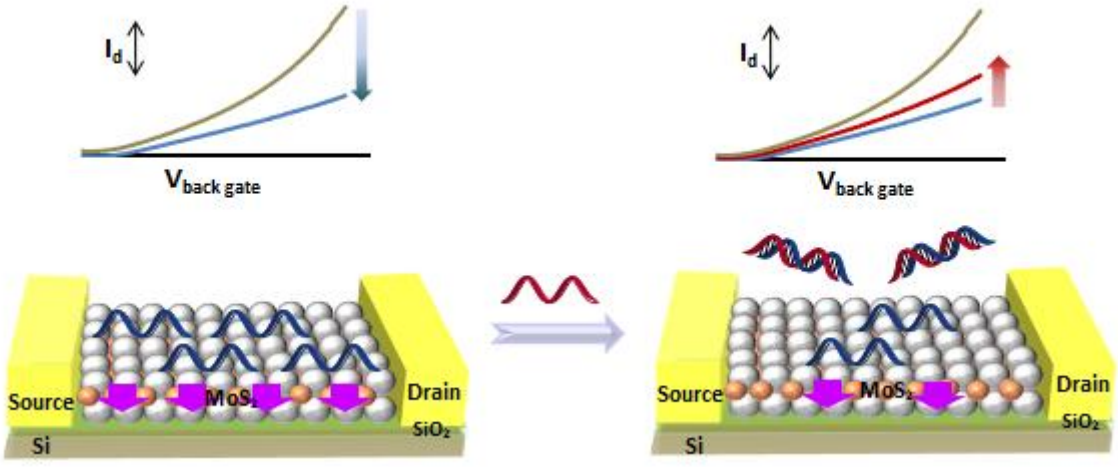

Scheme 1

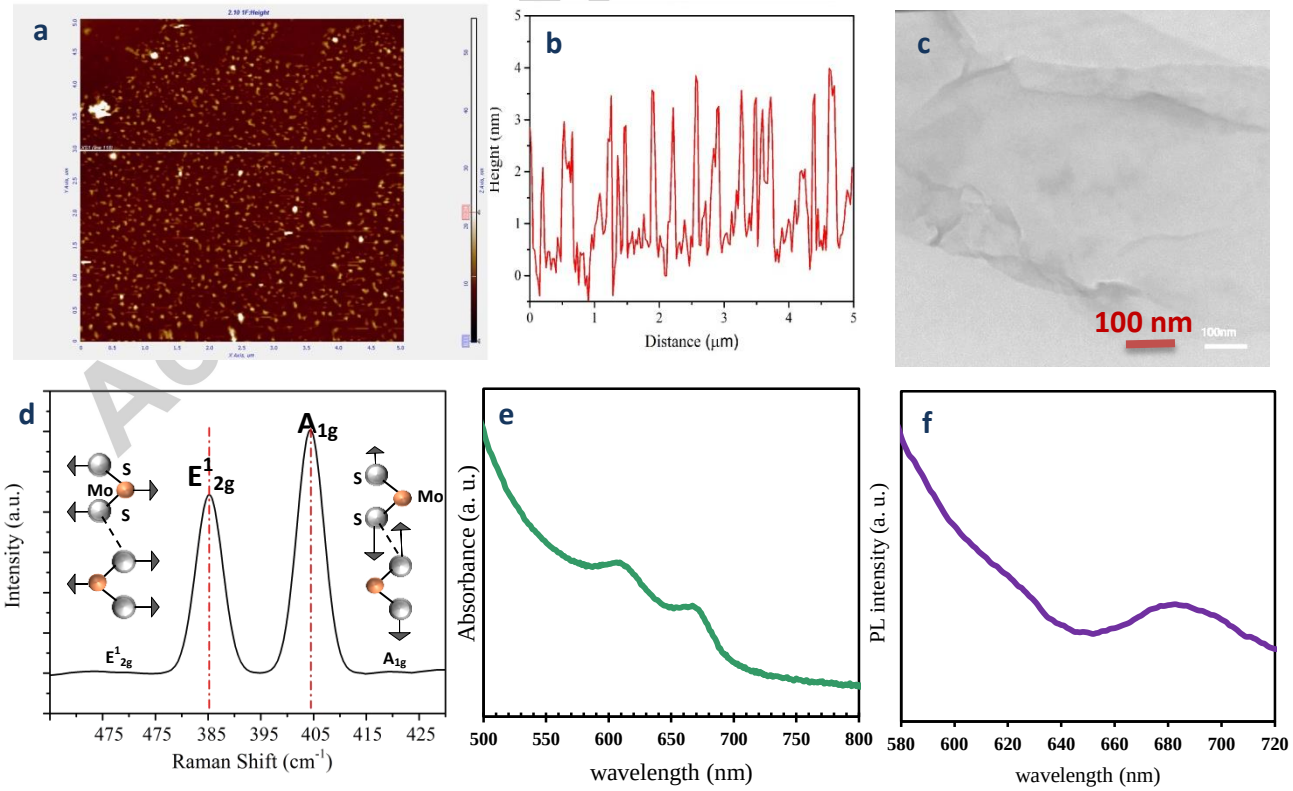

Figure 1

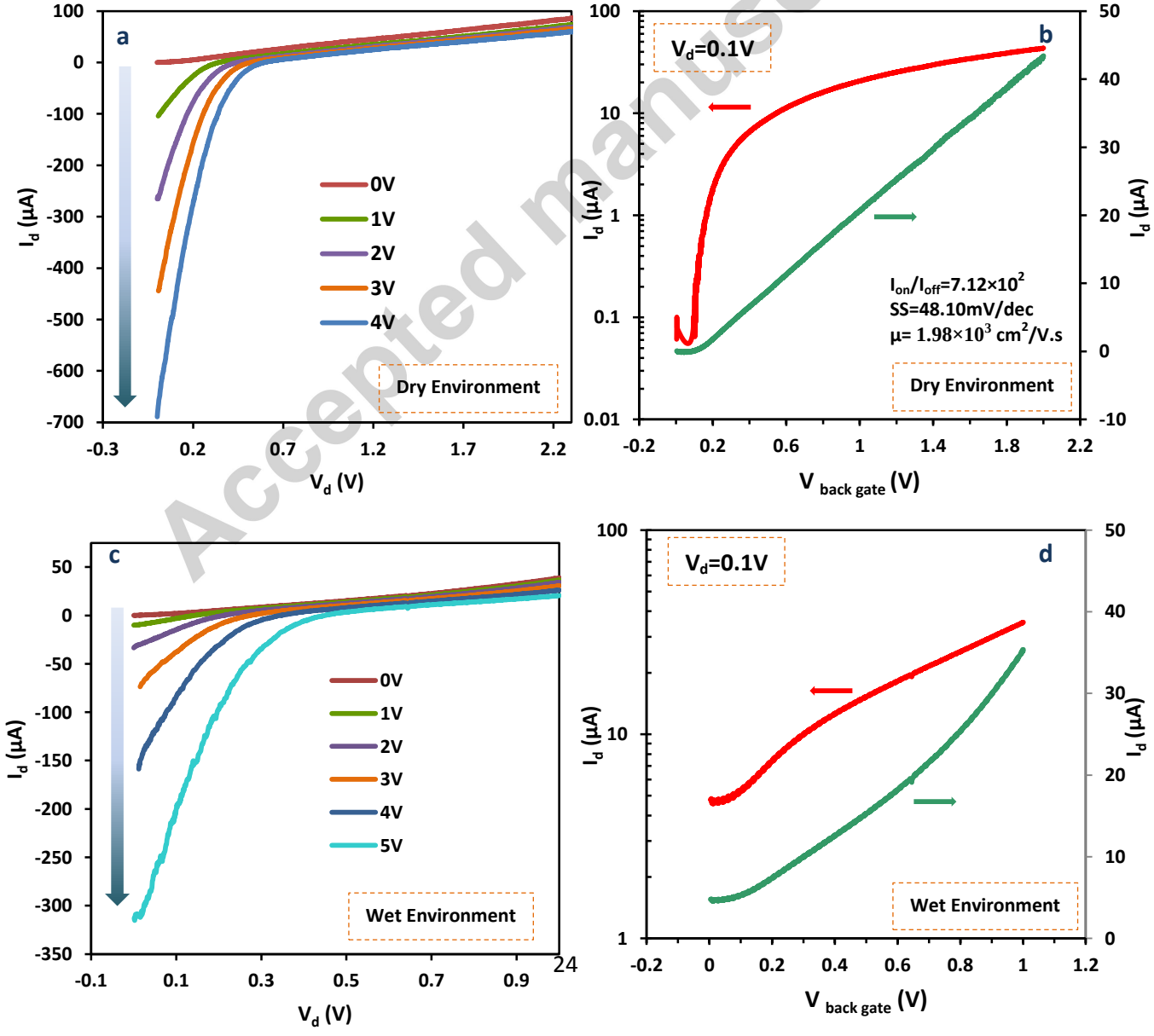

Figure 2

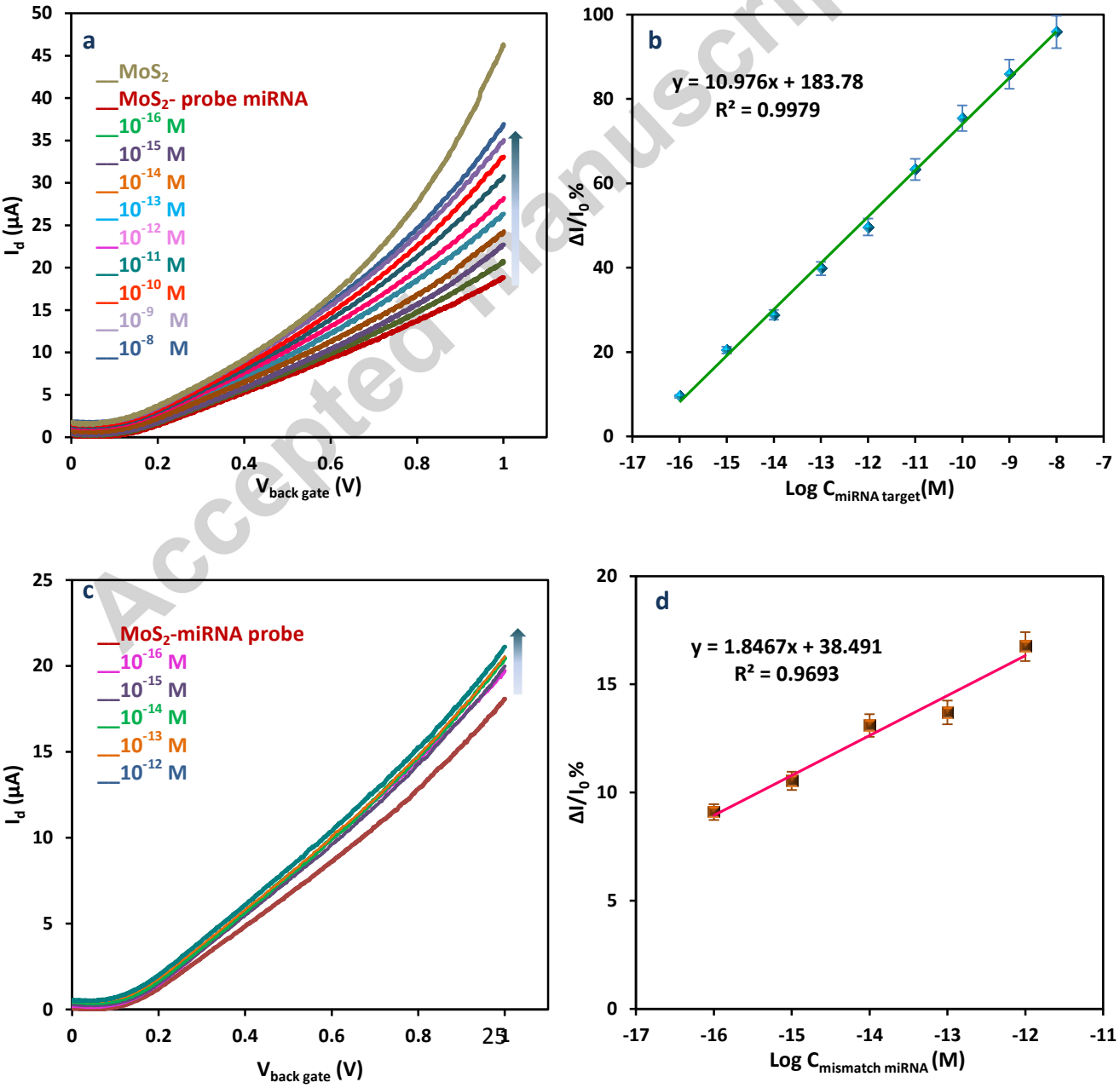

Figure 3

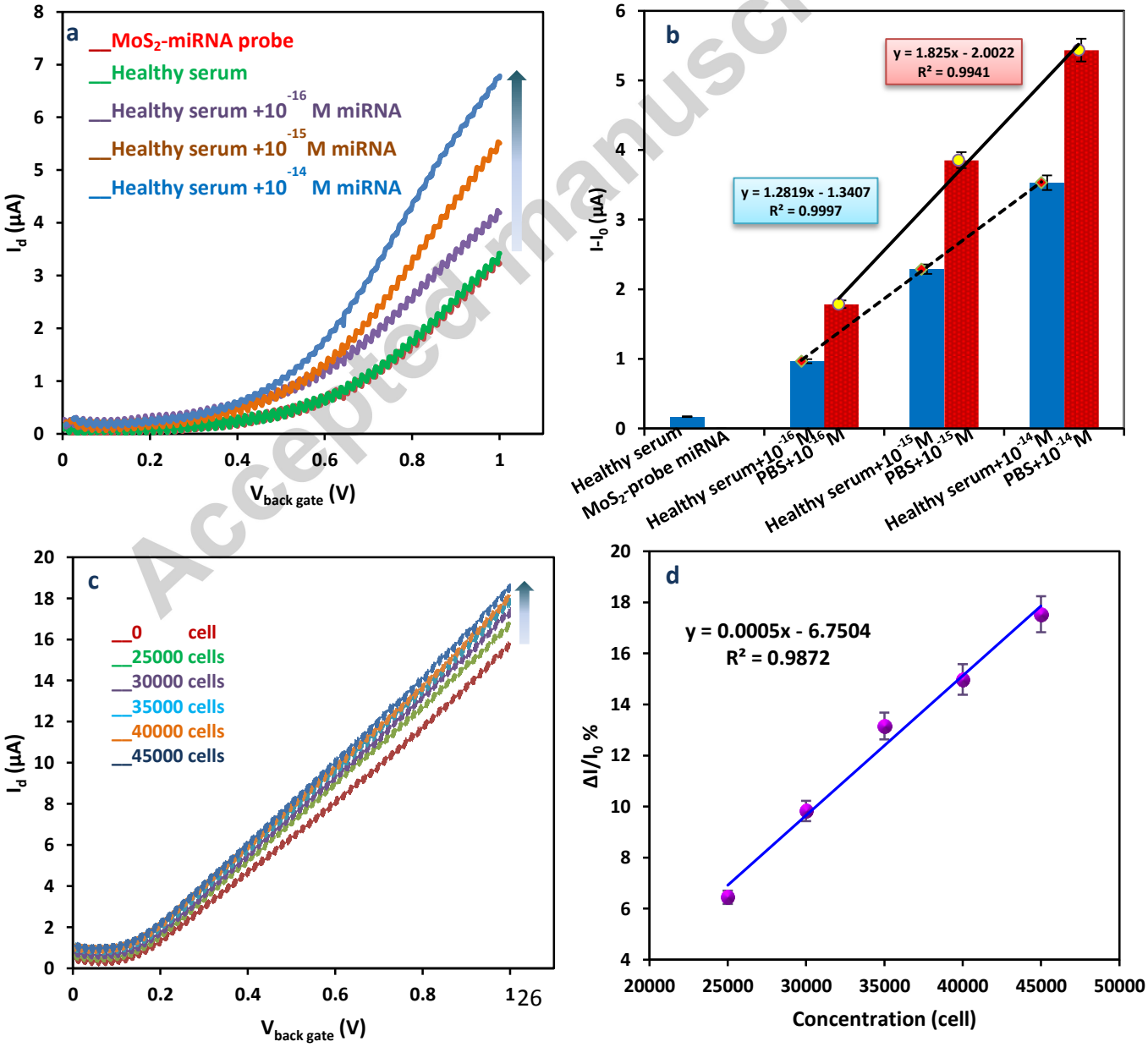

Figure 4

Graphical abstract

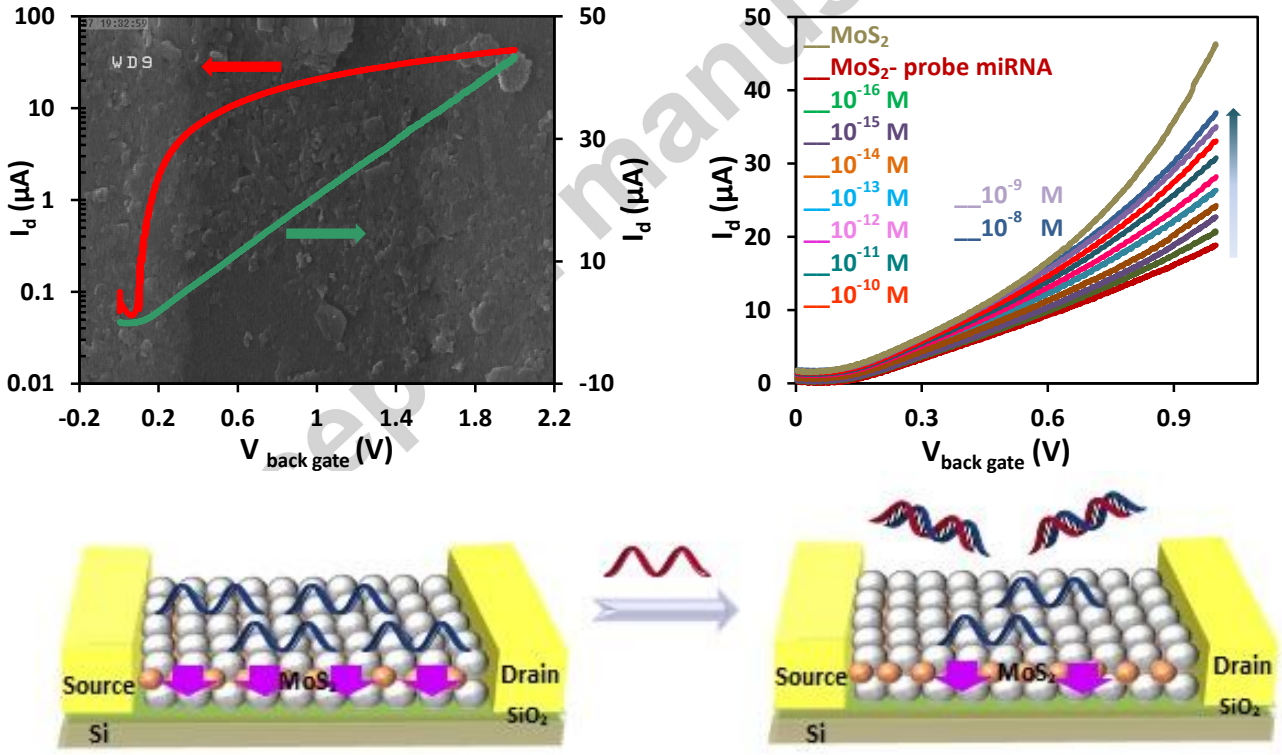

Highlights for review

Two dimensions MoS_2 nanosheets prepared through sequential solvent exchange method.

MoS_2 used for preparing of label free (FET) biosensor for miRNA155detection.

The DL of biosensor for miRNA detection was 0.03fM and concentration range 0.1fM-10nM.

Biosensor used for miRNA detection in real human serum and breast cancer cell-line.

Biosensor used to selective detection of fully matched *vs* one-base mismatch miRNA-155.